Combustion and Flame 158 (2011) 2428–2440

Contents lists available at ScienceDirect

Combustion and Flame

journal homepage: www.elsevier.com/locate/combustflame

Effects of water vapor addition on the laminar burning velocity of oxygen-enriched methane flames

A.N. Mazas [a,b,c,*], B. Fiorina [a,b], D.A. Lacoste [a,b], T. Schuller [a,b]

[a] CNRS, UPR 288 Laboratoire d'Energétique Moléculaire et Macroscopique Combustion (EM2C), Grande Voie des Vignes, 92295 Châtenay-Malabry, France
[b] Ecole Centrale Paris, Grande Voie des Vignes, 92295 Châtenay-Malabry, France
[c] Air Liquide, Centre de Recherche Claude-Delorme, Les Loges en Josas, BP 126, F-78350 Jouy-en-Josas, France

ARTICLE INFO

Article history:
Received 25 August 2010
Received in revised form 9 May 2011
Accepted 13 May 2011
Available online 21 June 2011

Keywords:
Oxy–fuel combustion
Oxygen-enhanced combustion
Steam addition
Water vapor addition
Laminar burning velocity
Conical flames

ABSTRACT

The effects of steam addition on the laminar burning velocity of premixed oxygen-enriched methane flames are investigated at atmospheric pressure. Experiments are carried out with an axisymmetric burner on which laminar conical flames are stabilized. A newly devised steam production system is used to dilute the reactants with water vapor. The oxygen-enrichment ratio in the oxidizer, defined as $O_2/(O_2 + N_2)$ (mol.), is varied from 0.21 (air) to 1.0 (pure oxygen). The equivalence ratio ranges from 0.5 to 1.5 and the steam molar fraction in the reactive mixture is varied from 0 to 0.50. For all compositions examined, the reactive mixture is preheated to a temperature T_u = 373 K. Laminar flame speeds are determined with the flame area method using a Schlieren apparatus. The deviations induced by stretch effects due to aerodynamic strain and flame curvature are assessed using Particle Imaging Velocimetry measurements and flame images, and these data are used to estimate the uncertainty of the flame speed measurements. The experiments are completed by numerical simulations conducted with the PREMIX code using different detailed kinetic mechanisms. It is shown that the laminar flame speed of $CH_4/O_2/N_2/H_2O_{(v)}$ mixtures features a quasi-linear decrease with increasing steam molar fraction, even at high steam dilution rates. Numerical predictions are in good agreement with experimental data for all compositions explored, except for low dilution rates $X_{H_2O} < 0.10$ in methane–oxygen mixtures, where the flame speed is slightly underestimated by the calculations. It is also shown that steam addition has a non-negligible chemical impact on the flame speed for methane–air flames, mainly due to water vapor high chaperon efficiency in third-body reactions. This effect is however strongly attenuated when the oxygen concentration is increased in the reactive mixture. For highly oxygen-enriched flames, steam can be considered as an inert diluent.

1. Introduction

Additives in flames are frequently used for various purposes, including pollutant emissions control, flame stabilization, promotion or inhibition of identified chemical reactions. It is well established that adding a diluent in a reactive mixture leads to significant changes in flame properties. The addition of a diluent can affect the combustion by the three following mechanisms: (a) a dilution effect caused by the reduction in reactants concentration in the reactive mixture; (b) a thermal effect due to the absorption by the additive of part of the heat released by the reaction, leading to a change in flame temperature; (c) a chemical effect owing to the activity of the additive that may alter some reactions paths. Those three mechanisms are concomitant and closely linked. For example, as chemical kinetics strongly depends on flame temperature, it is consequently difficult to analyze these effects separately.

Due to the increasing use of flue gas recirculation in combustion processes, water vapor and carbon dioxide are among the most common additives. While the effects of CO_2 dilution have already been thoroughly investigated (see e.g. Refs. [1–5]), the impact of steam addition has been the subject of a relatively limited number of studies, which are summarized below. In this work, the effects of water vapor addition on the laminar burning velocity of premixed oxygen-enriched methane flames are experimentally and numerically examined for various oxygen concentrations in the oxidizer. Varying the oxygen concentration in the oxidizer enables analysis of the sensitivity of water vapor dilution to flame temperature. Furthermore, the high reactivity of oxygen-enriched flames allows to investigate the effects of large steam dilution rates. Finally, studying the impact of steam addition on oxy–fuel flames is of practical interest since oxy–fuel combustion with flue gas

* Corresponding author at: Laboratoire EM2C, CNRS UPR 288, Grande Voie des Vignes, F-92295 Châtenay-Malabry Cedex, France.
E-mail address: antoine.mazas@airliquide.com (A.N. Mazas).

0010-2180/$ - see front matter © 2011 The Combustion Institute. Published by Elsevier Inc. All rights reserved.
doi:10.1016/j.combustflame.2011.05.014

recirculation receives a particular attention for its potential use for CO_2 capture and storage [6,7].

Addition of steam in the reactants can be used for various purposes. It was quickly identified as a successful way to lower pollutant emissions, including NO_x emissions, in gas turbines operating both in premixed and non-premixed modes [8–13]. It was then shown that steam addition in various combustible mixtures (natural gas, *n*-heptane, *iso*-octane) led to substantial reductions of NO_x emissions due to combined effects of flame temperature and oxygen atom concentration decrease [14,15]. Operating at constant adiabatic flame temperature, water vapor dilution was found to reduce NO_x levels by more than a factor of two compared to nitrogen dilution [16]. It was also observed that steam addition has a very limited impact on CO emissions for a fixed flame temperature [14,15].

The influence of steam as a fire inhibitor has also been recognized. Water vapor addition was found to be more effective at reducing the burning velocity of methane–air flames than the addition of other gaseous thermal agents (N_2 and CF_4) or chemical agents (CF_3Br), but less effective than the same mass of water mist [17]. These studies are however mainly based on numerical simulations; experiments were limited yet to small concentrations of added water vapor, with steam mass fractions typically lower than 0.02 [17,18]. This is mainly due to technical difficulties to seed the reactive flow with well-controlled high steam concentrations. Studies on inhibition of premixed flames by the means of various types of diluents can be closely linked to the present study because the reduction in laminar burning velocity can be used as a relevant indicator of an inhibiting agent effectiveness [19].

The effects of water vapor addition on flame extinction and ignition have also been examined. The initiation of laminar premixed H_2/air/H_2O and H_2/O_2/H_2O flames was numerically investigated and the critical conditions of propagation of the initial kernel were identified in terms of ignition energy and flame kernel radius [20,21]. Critical conditions of ignition and extinction for hydrogen and methane planar stretched flames were also measured and computed as a function of the water mass fraction in the oxidizer [22,23]. It was observed that steam addition favors extinction for both premixed and non-premixed flames, and reduces the flammability range. The chemical effect of steam addition in hydrogen–air and methane–air flames was mainly attributed to the chaperon efficiency of water in three body reactions. Experiments were also conducted by Le Cong and Dagaut [24] with a jet-stirred reactor operated at pressures $p_u = 1$ and 10 bar to further analyze the chemical effects of steam addition. Ignition delays and species concentrations were measured during the oxidation of hydrogen and methane with 10% (mol.) of water vapor and compared to computed results. It is shown that steam addition affects combustion kinetics mainly because of H_2O high third-body efficiency in the reaction $H + O_2 + M \rightleftharpoons HO_2 + M$.

Finally, the effects of steam addition on the laminar burning velocity have been examined with various experimental configurations. Burning velocities of hydrogen–air–steam mixtures were measured by Liu and MacFarlane [25] using conical flames, for steam molar fractions limited to $X_{H_2O} \leqslant 0.12$ and for unburned temperatures ranging from $T_u = 300$ to 523 K. Using a similar configuration, Koroll and Mulpuru [26] reported flame speed data of hydrogen–air–steam and hydrogen–oxygen–steam mixtures, featuring a wide range of steam concentrations. Laminar flame speeds of moist syngas mixtures were reported by Das et al. [27] using a counterflow twin-flame configuration. Spherical constant volume vessels were used by Shebeko et al. [28] and by Kuznetsov et al. [29] to investigate the flame speed evolution of steam-diluted mixtures at elevated pressure. Burning velocities of methane–air–steam flames were also determined by Babkin and V'yun [30] using spherically expanding flames in a constant volume vessel. Measurements were carried out for stoichiometric mixtures over a wide range of initial pressures $p_u = 1$–20 bar, at a fixed unburned gas temperature $T_u = 473$ K and for water vapor molar fractions varying from $X_{H_2O} = 0$ to 0.20. Burning velocities were deduced from direct photographs of the early stage of the flame kernel propagation. Results at atmospheric pressure show a linear decrease of the burning velocity when the water vapor molar fraction X_{H_2O} is increased, but data have not been reported yet for non-stoichiometric or oxygen-enriched mixtures.

Experiments and numerical simulations are conducted in this work to examine the effects of water vapor addition on the laminar burning velocity of oxygen-enhanced methane flames at atmospheric pressure. The objectives of this study are multiple.

1. An original technical solution for steam generation is presented. This system, based on a membrane permeation process, enables to accurately monitor the concentration of water vapor in the reactive mixture, and to cover a wide range of steam mass flow rates.
2. The second objective is motivated by the lack of data on fundamental aspects of steam diluted oxy–fuel flames. An experimental database is presented for laminar flame speeds of CH_4/O_2/N_2/H_2O mixtures at atmospheric pressure. Burning velocities are determined over wide ranges of equivalence ratios, oxygen-enrichment ratios and water vapor dilution rates.
3. This experimental database is completed by numerical simulations using different detailed kinetic mechanisms. Numerical results are compared to experimental data and used to analyze the respective contributions of dilution, thermal and chemical effects of steam addition.

The experimental facility and the steam production system are described in Section 2. The methodology used for the determination of the flame speed is then introduced in Section 3. Experimental data and numerical results are finally presented and discussed in Section 4.

2. Experimental facility and numerical tools

Experiments are conducted on an oxy–fuel combustion dedicated set-up, including heated gas feeding lines, a steam production apparatus and an axisymmetric burner on which steady conical laminar premixed flames are stabilized.

2.1. Experimental set-up

An overview of the experimental set-up is shown in Fig. 1. Methane (CH_4), oxygen (O_2) and nitrogen (N_2) gases (purity >99.99%) are supplied from an external network of tanks. The flow rates are regulated with mass flow controllers (Bronkhorst F-Series), calibrated with the related gas. The precision of the mass flow rates corresponds to ±2% of the set operating condition. Oxygen and nitrogen are premixed before being introduced as a carrier gas in a humidifier, which is described in the next SubSection 2.2. The O_2/N_2/H_2O mixture and the methane flow are then premixed before being introduced in an axisymmetric burner. A detailed view of the burner is shown in Fig. 2. Gases are injected in the lower part of the burner, which is filled with glass beads of different diameters (1–5 mm) to further reduce possible mixture non-homogeneities. The reactive mixture then flows successively through a perforated plate, a honeycomb structure and a refined metallic grid to obtain a laminar flow entering the inlet of a profiled converging nozzle. The burner can be equipped with three different converging nozzles of outlet diameters $d = 10$, 7 or 4 mm corresponding to contraction ratios of $\sigma = (D/d)^2 = 41$, 84 and

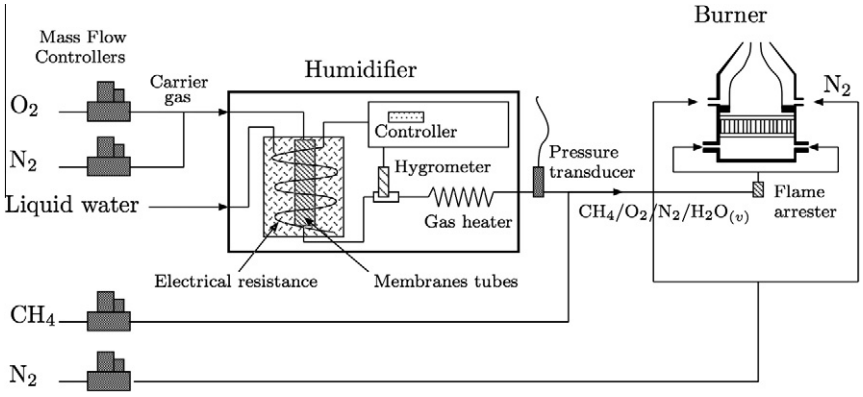

Fig. 1. Schematic of the experimental facility dedicated to premixed steam-diluted oxy–fuel combustion.

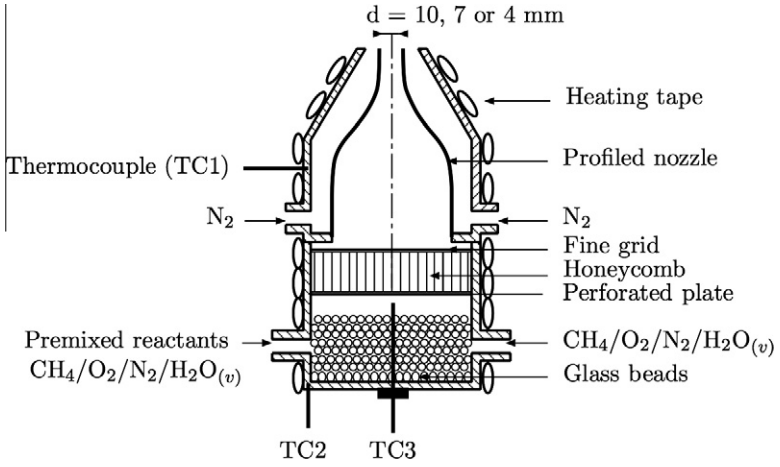

Fig. 2. Detailed schematic of the burner.

256. This converging nozzle is used to reduce the boundary layer thickness by accelerating the flow and to obtain a top hat velocity profile at the burner outlet. The burners of diameter $d = 10$ and 7 mm are used to stabilize conical methane–air flames and oxygen-enriched flames, for oxygen-enrichment ratios lower than $\Omega = O_2/(O_2 + N_2)$ (vol.) = 0.50. For larger oxygen-enrichment ratios, the burner is equipped with the nozzle of diameter $d = 4$ mm. A small co-flow of nitrogen surrounding the inner main nozzle may also be used to prevent potential external perturbations. In this study, this nitrogen co-flow was used only for non-preheated methane–air flames. It was not used for preheated mixtures to avoid undesirable cooling effects.

The temperature of all the components downstream the humidifier is controlled and set at the unburned gases temperature T_u to prevent water condensation. The burner temperature is regulated with an electrical heating tape (Vulcanic) and the homogeneity of the temperature field is monitored with thermocouples. A J-type thermocouple TC1 inserted in the burner body and a K-type thermocouple TC2 located at the basis of the burner are used to control the burner temperature. A third K-type thermocouple TC3 located immediately upstream the perforated plate is also used to measure the fresh mixture temperature T_u (Fig. 2).

The quality of the laminar flow obtained at the burner outlet was determined with time resolved pointwise measurements completed by two-dimensional snapshots of the velocity field in a vertical plane. Velocity profiles at the burner outlet were characterized using a small hot wire anemometry system (Dantec). Figure 3 shows that the axial velocity profile remains flat over

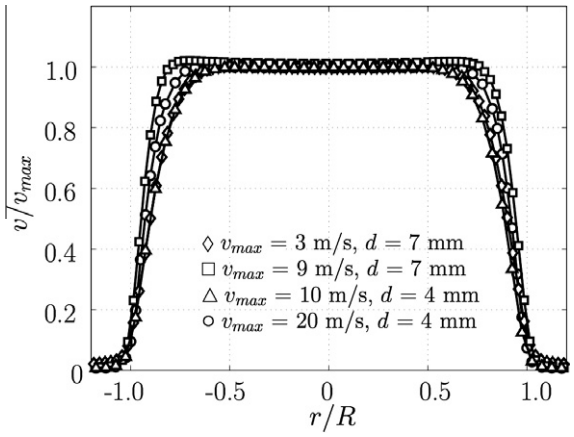

Fig. 3. Velocity profiles v/v_{max} at the burner outlet for various flow velocities and burner diameters $d = 7$ and 4 mm.

70% of the burner diameter. The RMS fluctuations are found to be less than 2.0% of the mean velocity, even for high velocities up to 20 m s^{-1}. This was completed by Particle Imaging Velocimetry (PIV) measurements, obtained with a 10 Hz-pulsed Nd:Yag laser (Continuum) and a set of cylindrical and spherical lenses, used to generate a 0.5 mm thick vertical laser sheet focused in the burner central plane. In these experiments, the flow is seeded with micronic zirconium dioxide ZrO_2 particles. The Mie scattering signal is

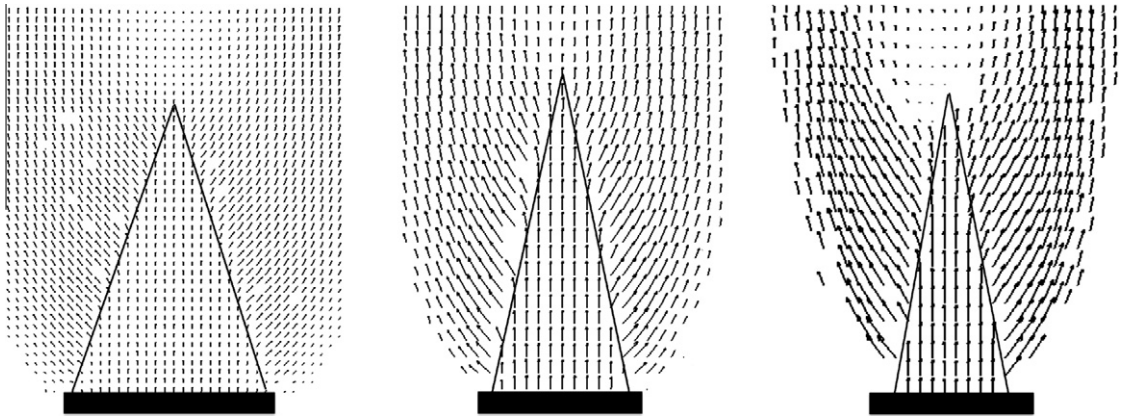

Fig. 4. PIV images of stoichiometric $CH_4/O_2/N_2$ flames for various oxygen-enrichment ratios Ω, at atmospheric pressure and ambient temperature. Left: $\Omega = 0.30$, converging nozzle diameter $d = 7$ mm; Center: $\Omega = 0.50$, converging nozzle diameter $d = 4$ mm; Right: $\Omega = 1.0$, converging nozzle diameter $d = 4$ mm. Only one velocity vector over four is shown here.

collected at the right angle onto a CCD camera (1600 × 1186 square pixels, Dantec Hi-Sense) equipped with a 200 mm lens (Nikkor) and with an interferential filter at the lasing wavelength $\lambda = 532$ nm. The post-processing of tomographic snapshot pairs is carried out with Dantec Flow Manager v4.1 software. Typical PIV images of stoichiometric $CH_4/O_2/N_2$ flames are shown in Fig. 4 for various oxygen-enrichment ratios $\Omega = O_2/(O_2 + N_2)$ (vol.) = 0.30, 0.50 and 1.0. The flow is uniform in the unburned gases in both radial and longitudinal directions. The axial velocity gradient measured between the burner outlet and the flame tip is typically lower than 10 s^{-1}.

Laminar flame speeds are determined with Schlieren images obtained with a classical Z-arrangement set-up. The Schlieren apparatus includes converging lenses of 100 mm diameter with large focal lengths $f = 1000$ mm, plane mirrors and vertical knives (Ealing) to highlight horizontal density gradients [31]. Schlieren images are recorded with a video CCD camera (768 × 576 square pixels, Pulnix), equipped with a variable speed shutter and a 100–300 mm lens (Cosina) to zoom in the flame region. This is completed with flame chemiluminescence images recorded with another CCD camera without specific filter. Typical Schlieren images and chemiluminescence images are shown in Fig. 5 for stoichiometric oxygen-enriched flames, anchored on the $d = 7$ and 4 mm burners respectively. Chemiluminescence images of steam diluted flames are also shown in Fig. 6. The flames obtained are straight-sided cones, ensuring that the flame propagation speed is uniform over the main part of the reaction zone [32].

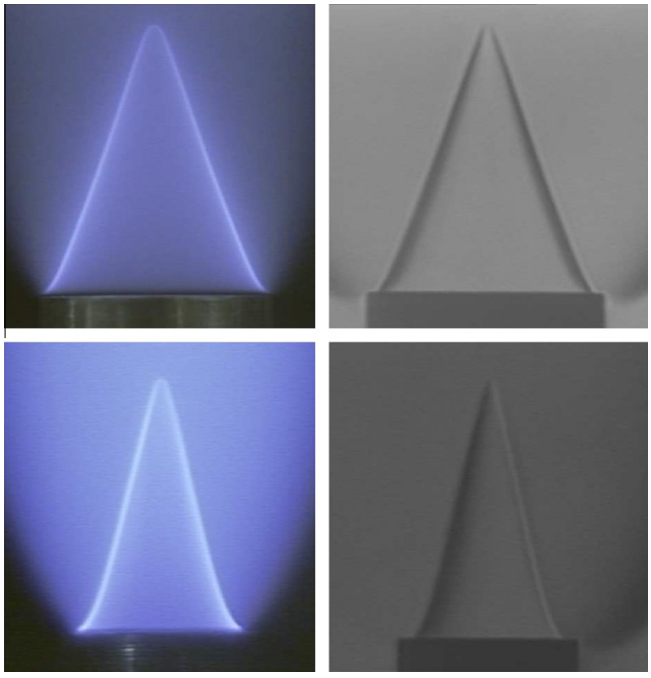

Fig. 5. Typical chemiluminescence photograph (left) and corresponding Schlieren image (right) of $CH_4/O_2/N_2$ flames. Top: $\Omega = 0.30$, $\phi = 1.0$; bottom: $\Omega = 1.0$, $\phi = 1.0$.

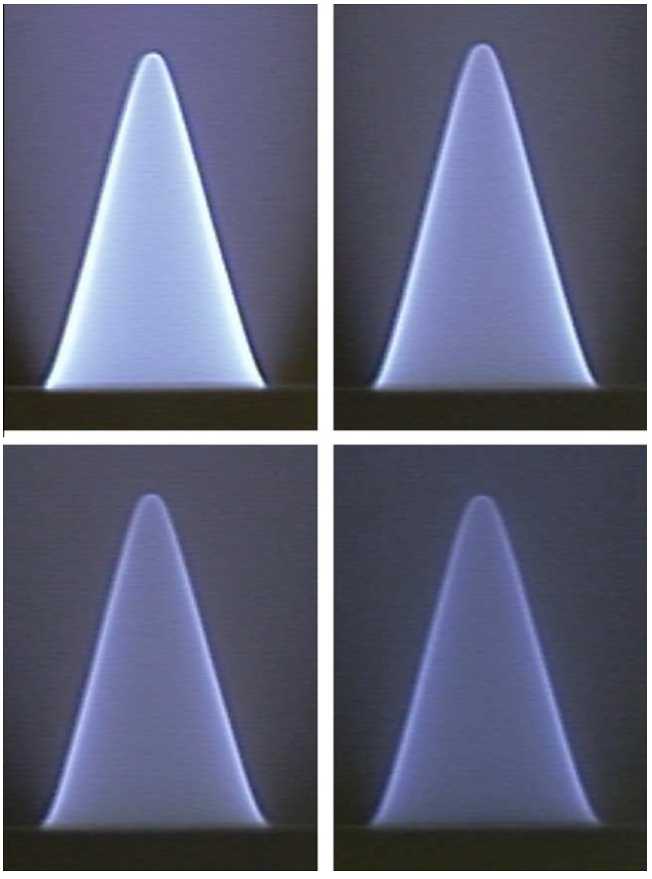

Fig. 6. Chemiluminescence images of $CH_4/O_2/N_2/H_2O$ flames, for $\Omega = 0.50$ and $\phi = 1.5$. From top to bottom, from left to right: $X_{H_2O} = 0$, $X_{H_2O} = 0.09$, $X_{H_2O} = 0.14$, $X_{H_2O} = 0.18$.

2.2. Steam production system

Water vapor is produced with a custom-built device derived from a Cellkraft P-50 humidifier. Steam addition is based on the humidification of the carrier gas by transfer of water vapor through Nafion® membranes (DuPont). The carrier gas flows in the membrane tubes, which are immersed in demineralized liquid water heated with electrical resistances at a temperature T_{lw}. At the tube exit, the carrier gas is saturated with steam and the dew point temperature T_{dew} of the humidified mixture is measured with a high precision humidity sensor (Vaisala Humicap Series HMT 330). A closed loop control of humidity based on the measured dew point temperature T_{dew} at the tube outlet is used to regulate the temperature of liquid water T_{lw} in which the membrane tubes are immersed. This temperature T_{lw} is adjusted by the controller to match the desired dew point of $O_2/N_2/H_2O$ mixtures obtained at the humidifier outlet. The steam molar fraction $X^*_{H_2O}$ in this mixture can then be inferred from the steam partial pressure p_{H_2O}, given by the saturation vapor pressure at the dewpoint temperature $p_{sat}(T_{dew})$, and from the humidifier inner pressure p_h, measured with a high temperature pressure transducer (Huba Control) at the humidifier outlet:

$$X^*_{H_2O} = \frac{p_{H_2O}}{p_h} = \frac{p_{sat}(T_{dew})}{p_h} \quad (1)$$

The performances of this humidifier were validated for a selected number of operating conditions representative of wet mixture compositions explored in the present study. These conditions are shown in Table 1. For these validation tests, air is used as a carrier gas, with mass flow rates successively set to $\dot{m}_{cg} = 776.3$ and 2329.0 g h^{-1}. The dew point temperature is also increased from $T_{dew} = 320$ to 350 K, corresponding to steam molar fractions $X^*_{H_2O} = 0.10$ and 0.42, respectively. The steam mass flow rates are determined by measuring the mass of water removed from the tank of liquid water. Measured steam mass flow rates are plotted as a function of time in Fig. 7 and are compared with predictions obtained with Eq. (1). These measurements are found to be in good agreement with theoretical predictions with a relative precision lower than 1%. It can be concluded from the humidifier linear operation and from the repeatability of these tests that the steam concentration is stable and accurately controlled.

2.3. Numerical simulations

Experiments are completed by simulations of one-dimensional, freely propagating, unstretched, adiabatic, laminar, premixed flames using the PREMIX code of the CHEMKIN package [33]. Two different detailed kinetic mechanisms are tested including the GRI-mech 3.0 mechanism [34] and a mechanism developed by Le Cong and Dagaut for methane oxidation in the presence of steam [24]. The GRI mechanism is commonly used for modeling the combustion of methane and natural gas, and has been validated for a wide range of equivalence ratios, unburned temperatures and pressures. It includes 53 species – with C1 to C3 molecules – involved in 325 elementary chemical reactions [34]. The second mechanism was recently developed to specifically include chemical effects of water vapor addition in hydrogen and methane combustion. It consists of 99 chemical species involved in 743 reactions and incorporates C1 to C6 molecules.

Table 1
Comparison of measured and predicted steam mass flow rates for various operating conditions. From left to right: Carrier gas (air) mass flow rate, humidifier pressure, dew point temperature, steam molar fraction, experimental and theoretical steam mass flow rates, relative difference.

$\dot{m}_{cg}$ (g/h)	p_h (mbar)	T_{dew} (K)	X_{H_2O}	$\dot{m}_{H_2O}$ (g/h)		Δ (%)
				Exp.	Theor.	
776.3	1010	320	0.10	56.2	56.1	0.1
2329.0	1010	320	0.10	166.8	168.4	−0.6
776.3	1217	350	0.42	254.6	253.0	1.0
2329.0	1692	350	0.42	474.2	475.6	−0.3

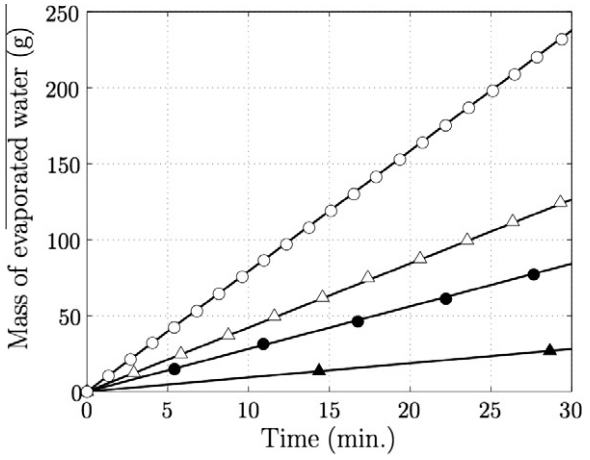

Fig. 7. Measured (symbols) and predicted (lines) mass of evaporated water as a function of time for different dew point temperatures T_{dew} and carrier gas mass flow rates $\dot{m}_{cg}$. (▲) $T_{dew} = 320$ K and $\dot{m}_{cg} = 776.3$ g/h; (•) $T_{dew} = 320$ K and $\dot{m}_{cg} = 2329$ g/h; (△) $T_{dew} = 350$ K and $\dot{m}_{cg} = 776.3$ g/h; (o) $T_{dew} = 350$ K and $\dot{m}_{cg} = 2329$ g/h.

Simulations are also conducted with a virtual species, hereafter designated as Virt-H_2O, to investigate the effects of water vapor dilution on combustion chemistry. This virtual species Virt-H_2O is added in both detailed mechanisms. It is assigned the same molecular structure, and the same thermodynamic and transport properties as water vapor. This virtual species Virt-H_2O does however not appear in the elementary reactions of the kinetic mechanisms. Thereby, numerical calculations conducted with Virt-H_2O highlight dilution and thermal effects of steam addition only. For a given mixture composition, the chemical effects of steam addition can then be isolated by comparison of the results obtained with real $CH_4/O_2/N_2/H_2O$ mixtures and the ones obtained with artificial $CH_4/O_2/N_2$/Virt-H_2O mixtures [2,4,24,35].

3. Flame speed measurement methodology

The laminar burning velocity s^o_u is the velocity at which a laminar, steady, plane, unstretched, adiabatic flame moves relative to the unburned premixed gas in the direction normal to the flame surface [36]. It is however established that a flame that perfectly matches all these requirements is difficult to obtain and different experimental configurations have been developed to generate flows approaching these conditions [37]. These configurations have been continuously improved and a particular attention was paid to correct thermal, stretch and curvature effects that are known to affect the laminar burning velocity [38–49]. The suitable experimental configuration for flame speed measurements mainly depends on the range of burning velocities to be explored. Compared to air combustion, it is established that highly oxygen-enriched premixed flames (a) feature significantly higher burning velocities [32], (b) are subject to flame instabilities [50,51], and (c) are characterized by a high sensitivity to detonation [52–54]. These properties considerably constrain the choice of an appropriate configuration for the measurement of oxy–fuel flames burning velocities and make the conical flame

method a reliable and safe solution for laminar premixed oxy–fuel flames studies [26,32,55].

In this study, the flame speed measurement is an area-weighted average over the entire flame surface. Assuming that the whole reactive mixture injected in the burner is consumed across the premixed flame front (see Fig. 8), the area-weighted average laminar flame speed s_u is given by the mass balance equation:

$$\dot{m} = \rho_u s_u A_f \tag{2}$$

where $\dot{m}$ is the reactants mass flow rate, ρ_u the unburned gas density and A_f the flame surface area. Since the laminar burning velocity s_u^o is defined relative to the unburned gases, the appropriate area A_f is the upstream boundary of the preheat zone, which can be determined by the Schlieren technique [31,32,36,56–58]. The flame area A_f is determined from the Schlieren images with an edge detection program based on Sobel operator. For each operating condition, 20 Schlieren images are typically recorded. The area A_f is averaged over these 20 images, assuming the flame is axisymmetric around the burner axis. The relative root-mean-square deviation of the flame surface area determined with the set of Schlieren images is less than 2% of the mean value A_f.

Conical flames stabilized on the rim of a cylindrical burner are not rigorously adiabatic, and are affected by stretch effects. Heat losses are difficult to evaluate. The burner wall temperature was measured close to the flame with a K-type thermocouple of diameter 0.25 mm. The burner temperature reaches about 473 K for methane–oxygen flames at atmospheric pressure. Since only a small fraction of the flame surface lies close to solid boundaries and considering the reduced thickness of the burner outlet (0.5 mm), heat losses at the burner rim can be neglected compared to the total heat release. Furthermore, quenching effects at the flame foot are reduced due to the increase of the flame temperature when the oxygen-enrichment ratio is increased. It is observed on chemiluminescence and Schlieren images shown in Figs. 5 and 6 that the flame front edge starts at the immediate vicinity of the burner rim. Radiative heat losses are likely to increase due to the contributions of steam vibrational bands in the infra-red range, but this effect needs to be considered only at elevated pressure.

Premixed conical flames are also affected by stretch effects due to aerodynamic straining and flame curvature [48]. Consequently, an estimation of the difference between the reported flame speed s_u, which is measured with the methodology described below, and the unstretched laminar flame speed s_u^o is needed. Aerodynamic straining of the flame front is first examined. Figure 3 shows that the velocity profile at the burner outlet is nearly uniform and PIV measurements presented in Fig. 4 show that the velocity gradients in radial and longitudinal directions are limited. Tangential velocity profiles along the flame front, extracted from PIV measurements, are also plotted in Fig. 9 for various oxygen-enrichment ratios $\Omega = 0.30$, 0.50 and 1.0. The velocity gradients along the flame front lies typically within 50 s^{-1} for $\Omega = 0.30$, 80 s^{-1} for $\Omega = 0.50$

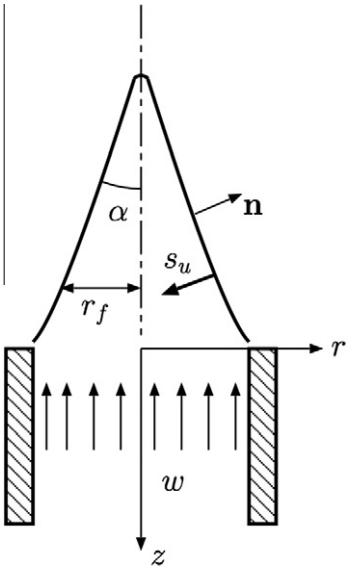

Fig. 8. Schematic of a conical flame stabilized over an axisymmetric burner.

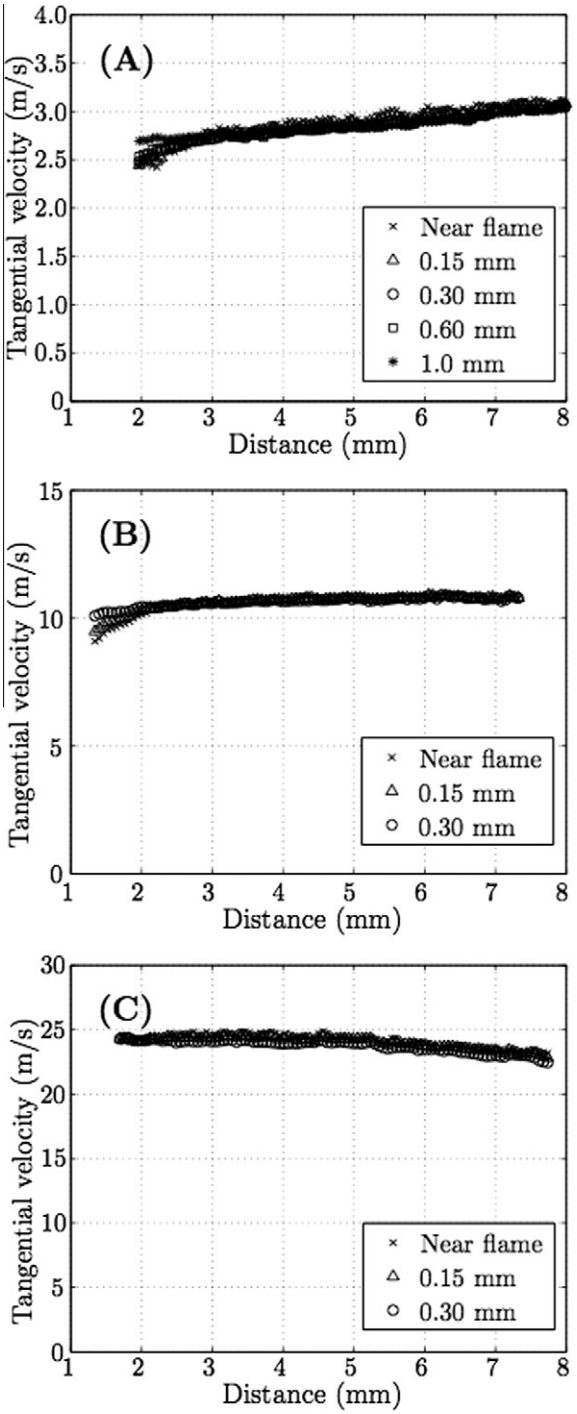

Fig. 9. Velocity profiles along the flame front of stoichiometric $CH_4/O_2/N_2$ flames, for various oxygen-enrichment ratios. (A) $\Omega = 0.30$, $\phi = 1.0$; (B) $\Omega = 0.50$, $\phi = 1.0$; (C): $\Omega = 1.0$, $\phi = 1.0$. Tangential velocities are reported for various distances to the flame front in normal direction towards the unburned gases.

and 200 s^{-1} for $\Omega = 1.0$. It is also observed that the tangential velocity gradient measured near the flame anchoring point is limited, in accordance with the results reported by Choi and Puri [59], and its effect on the measured flame speed is minimal. Stretch effects due to aerodynamic straining are thus limited in the present configuration.

Here, the stretch effects affecting the conical flames are mainly due to flame curvature, along the flame front and at the flame tip. As shown in Fig. 5, the round shape of the flame tip observed for methane–air flames is strongly reduced when the oxygen-enrichment ratio is increased. Oxygen-enriched flames feature sharp tips, especially in lean and near-stoichiometric conditions. Furthermore, the tip area is negligible compared to the total flame surface, that is why stretch effects due to tip curvature will not be considered here. The curvature of the reaction zone is calculated in the plane ($\mathbf{e}_\theta$, $\mathbf{n}$), where $\mathbf{e}_\theta$ and $\mathbf{n}$ are respectively the unit vector in the azimuthal direction and the unit vector normal to the flame front.

An error estimate due to stretch effects is conducted using the expression of the ratio s_u/s_u^o derived by Sun et al. [60] for a curved flame propagating in a non-uniform flow field. This estimate provides a confidence interval in the flame speed measurement methodology. For steady adiabatic non-equidiffusive flames, the ratio s_u/s_u^o is given by:

$$\frac{s_u}{s_u^o} = 1 + \frac{\mathrm{Ze}}{2}\left(\frac{1}{\mathrm{Le}} - 1\right)\frac{\alpha^o \kappa \delta_T^o}{s_u^o} + c\delta_T^o \tag{3}$$

where $\mathrm{Ze} = E_a(T_b^o - T_u)/\left[R(T_b^o)^2\right]$ is the Zeldovitch number, Le the Lewis number of the reactive mixture, κ the global stretch rate, δ_T^o the thermal flame thickness, c the flame curvature and α^o a factor accounting for the thermal expansion effect, with $\alpha^o = 1 + \ln[\sigma^o + (1-\sigma^o)e^{-1}]$ where $\sigma^o = T_u/T_b^o = \rho_b^o/\rho_u$. In the previous equation, E_a denotes the overall activation energy, R the universal gas constant, T and ρ the temperature and the density respectively; the subscripts u and b refer to properties associated with unburned and burned gas respectively and the superscript o indicates flow properties relative to one-dimensional unstretched flames. The ratio s_u/s_u^o is calculated for conical flames with various oxygen-enrichment ratios, representative of the present experimental configuration. The quantities T_b^o, Ze, Le, α^o and δ_T^o can be extracted from numerical simulations of one-dimensional adiabatic unstretched flames using the procedure suggested in Ref. [60]. Considering a small change in the nitrogen concentration to vary the temperature of the burned gases T_b^o, the activation energy can be obtained from:

$$E_a = -2R\,\frac{\partial \ln(\rho_u s_u^o)}{\partial(1/T_b^o)} \tag{4}$$

Here, this quantity was numerically determined from the results obtained with the PREMIX code, used with the GRI-mech 3.0, by varying the oxygen-enrichment ratio Ω. Similarly, the thermal flame thickness is estimated using the gradient of the calculated temperature profile:

$$\delta_T^o = \frac{T_b^o - T_u}{(dT/dx)_{max}} \tag{5}$$

The Lewis number of the mixture is estimated following the analysis proposed in Ref. [61] and ranges between $\mathrm{Le}_{\mathrm{CH_4}}$ and $\mathrm{Le}_{\mathrm{O_2}}$, both quantities being close to unity. For steady conical flames, the stretch rate κ can be expressed in the cylindrical coordinate system (r, θ, z) as [48]:

$$\kappa(r,\theta,z) = -\left(\frac{\sin\alpha}{r}\frac{\partial}{\partial r}(rw\cos\alpha) + \cos\alpha\frac{\partial}{\partial z}(w\cos\alpha)\right) \tag{6}$$

In this expression, w is the vertical component of the reactants mixture velocity and α the flame angle with respect to the flow direction, as shown in Fig. 8.

Neglecting flame curvature effects at the flame tip and at the flame basis in the vertical plane (r, z), Eq. (6) reduces to:

$$\kappa(r_f) = -\frac{w\sin(2\alpha)}{2r_f} \tag{7}$$

where r_f is the local flame radius in the cylindrical coordinate system. One can then define an area-weighted average stretch $\bar{\kappa}$ over the flame surface A_f:

$$\bar{\kappa} = \frac{1}{A_f}\int_{A_f} -\frac{w\sin(2\alpha)}{2r}dS = -\frac{w\sin(2\alpha)}{R} = \kappa\left(r_f = \frac{R}{2}\right) \tag{8}$$

where R is the radius of the conical flame basis. It is worth noting that the area-weighted average stretch $\bar{\kappa}$ is equal to the local stretch calculated at a radial distance $r = R/2$. Similarly, an area-weighted average curvature $\bar{c}$ can be defined:

$$\bar{c} = \frac{1}{A_f}\int_{A_f} c(r)dS = \frac{1}{A_f}\int_{A_f}\frac{1}{r\cos(\alpha)}dS = c\left(r_f = \frac{R}{2}\right) \tag{9}$$

Eqs. (8) and (9) suggest that the values of the local stretch $\kappa(r = R/2) = \bar{\kappa}$ and of the local curvature $c(r = R/2) = \bar{c}$ can be seen as global flame parameters useful for the analysis of stretch effects on the properties of conical laminar flames. The flame parameters required to estimate the flame speed ratio s_u/s_u^o given by Eq. (3) are presented in Table 2, for various oxygen-enrichment ratios Ω ranging from 0.21 (air) to 1.0 (pure oxygen). All these parameters were calculated using the PREMIX code with the GRI-mech 3.0 mechanism, except $\bar{\kappa}$ and $\bar{c}$ that were measured. It is found that the absolute value of the area-weighted average stretch $\bar{\kappa}$ increases when the oxygen-enrichment ratio is increased. This increase is due to the increase of the flow velocity and to the decrease of the burner diameter, needed to avoid flame instabilities. It is also observed that the thermal flame thickness δ_T^0 is significantly reduced when the oxygen-enrichment ratio is increased. This decrease strongly moderates the curvature effects on the flame speed. Finally, the relative difference between the measured flame speed and the unstretched laminar flame speed due to combined aerodynamic and curvature stretch effects remains limited. It is found to be within 15% for methane–air flames and within 10% for methane–oxygen flames.

Only raw data will be presented in Section 4 without correction by this estimate. The analysis conducted here shows that the uncertainty on burning velocity measurements due to stretch effects reduces for the oxygen-enriched mixtures considered in this study.

Table 2
Geometrical characteristics and computed flame parameters of stoichiometric $CH_4/O_2/N_2$ mixtures, for various oxygen-enrichment ratios $\Omega = X_{O_2}/(X_{O_2} + X_{N_2})$.

Ω	ϕ	T_b^o (K)	Ze	$\mathrm{Le}_{\mathrm{CH_4}}$	$\mathrm{Le}_{\mathrm{O_2}}$	α^o	$\bar{\kappa}$ (s^{-1})	δ_T^o (mm)	$\bar{c}$ (mm^{-1})
0.21	1.0	2261	8.9	0.95	1.10	0.25	−216	0.41	0.42
0.30	1.0	2548	10.7	0.93	1.12	0.22	−1278	0.24	0.59
0.50	1.0	2825	12.3	0.91	1.19	0.19	−3997	0.14	1.0
1.00	1.0	3060	13.2	0.84	1.68	0.16	−9993	0.10	1.1

4. Results and discussion

Laminar flame speeds of $CH_4/O_2/N_2/H_2O_{(v)}$ mixtures are measured for different operating conditions. The parameters examined in this work are (a) the oxygen-enrichment ratio in the oxidizer Ω:

$$\Omega = X_{O_2}/(X_{O_2} + X_{N_2}) \quad (10)$$

where X_k is the molar fraction of the species k, (b) the steam molar fraction X_{H_2O} in the reactive mixture and (c) the mixture equivalence ratio ϕ, defined as:

$$\phi = \left(\frac{\dot{m}_{CH_4}}{\dot{m}_{O_2}}\right) \Big/ \left(\frac{\dot{m}_{CH_4}}{\dot{m}_{O_2}}\right)_s \quad (11)$$

In this expression $(\dot{m}_{CH_4}/\dot{m}_{O_2})_s$ indicates the stoichiometric fuel-to-oxygen mass ratio. All experiments are conducted for a constant unburned gas temperature T_u = 373 K, except for the cases of dry and wet CH_4/air mixtures where the gas inlet temperature is set either to T_u = 298 K or to T_u = 473 K, to compare the results with existing experimental data [30,47]. All these temperatures are controlled with a precision of ±2 K. Experimental results are presented with vertical error bars of ±5% indicating the uncertainty in the flame speed determination with the present methodology.

4.1. Validation of the experimental methodology

The experimental methodology is first validated with well documented CH_4/air flames at T_u = 298 K and at atmospheric pressure. Laminar flame speeds are measured for mixture equivalence ratios varying from ϕ = 0.8 to 1.5, as shown in Fig. 10. Leaner CH_4/air flames cannot be stabilized with this set-up. The present results are compared with reference measurements of stretch-corrected flame speeds obtained with various experimental configurations. Vagelopoulos and Egolfopoulos [47] measured CH_4/air laminar flame speeds with counterflow flames in a near-zero strain-rate state, using Laser Doppler Velocimetry. Burning velocities measurements were obtained by Hassan et al. [62] with outwardly propagating spherical laminar premixed flames at constant pressure. Bosschaart and de Goey [63] used the heat flux method to stabilize flat adiabatic flames over a thin perforated plate burner, while Dong et al. [64] used a stagnation flow configuration with a Digital Particle Image Velocimetry system to determine CH_4/air laminar flame speeds. The results of the present work are in good agreement with these data. In lean and near-stoichiometric conditions, the data are in accordance with the reference measurements within the error bars. For rich conditions, the data scattering increases slightly. The measured flame speeds are found to be close to the results of Vagelopoulos and Egolfopoulos [47]. Furthermore, a good agreement between measured and computed burning velocities is noted, experimental results being lower than numerical calculations presumably due to heat losses at the burner rim.

The dependence of the flame speed on steam addition in methane flames is now investigated. Figure 11 shows the evolution of the burning velocity of stoichiometric CH_4/air/$H_2O_{(v)}$ mixtures when the steam molar fraction is increased from X_{H_2O} = 0 to 0.20, at T_u = 473 K. Also plotted are the computed burning velocities for reactive mixtures diluted respectively with steam and with the virtual species Virt-H_2O introduced in Section 2.3. The laminar flame speed decreases with increasing water vapor molar fraction. This decrease is found to be linear when the steam molar fraction X_{H_2O} is varied between 0 and 0.10. Numerical calculations reproduce accurately the experimental results. One can also observe a significant difference between the calculated flame speeds obtained with steam dilution and those obtained with the virtual species. The relative difference $\eta = (s_u(X_{Virt\text{-}H_2O}) - s_u(X_{H_2O}))/s_u(X_{H_2O})$ reaches 29% for $X_{H_2O} = 0.20$, highlighting chemical effects of steam addition in these conditions. This point is discussed further in the paper. The evolution of the ratio $s_u(X_{H_2O})/s_u(X_{H_2O} = 0)$ is plotted in Fig. 11 and the results are compared with data obtained by Babkin and V'yun with spherically expanding flames in a constant volume vessel [30]. A good agreement is found between these data, the present measurements

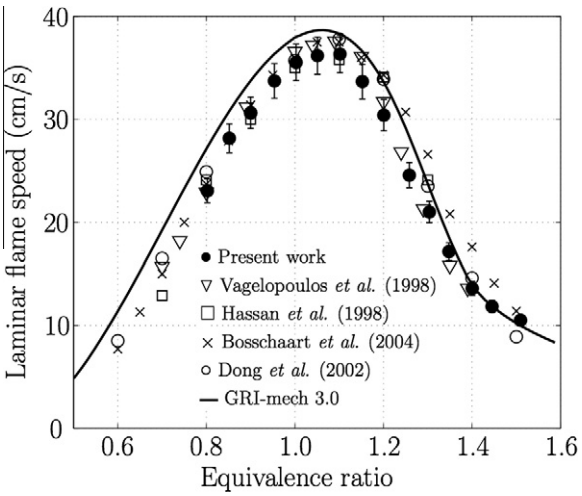

Fig. 10. Experimental (symbols) and computed (lines) laminar flame speeds of CH_4/air mixtures, at T_u = 298 K and atmospheric pressure.

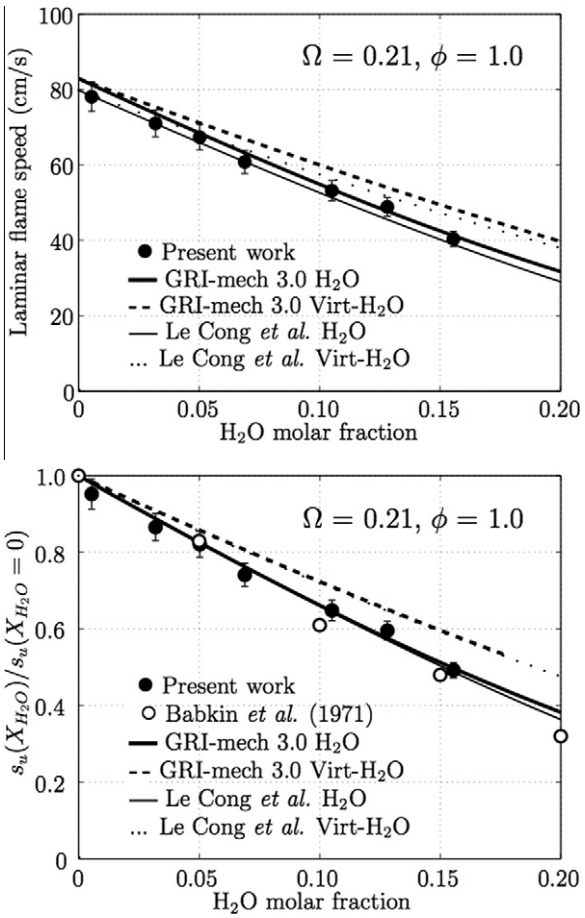

Fig. 11. Top: Experimental (symbols) and computed (lines) laminar flame speeds of stoichiometric CH_4/air/H_2O mixtures, at T_u = 473 K and atmospheric pressure. Bottom: laminar flame speed ratio $s_u(X_{H_2O})/s_u(X_{H_2O} = 0)$ in the same conditions.

and the numerical predictions obtained with the two detailed kinetic mechanisms. Results presented in Fig. 10 for dry methane–air mixtures and those presented in Fig. 11 for methane–air–steam mixtures validate the experimental methodology developed in the present study for laminar flame speed measurements in wet conditions. This methodology yields results in agreement with existing data obtained with different experimental techniques and numerical predictions within about 5% accuracy.

4.2. Effects of steam addition on the burning velocity of oxygen-enriched mixtures

In this section, burning velocity measurements of oxygen-enriched methane flames diluted with steam are reported for the first time. While the effects of steam addition on the flame speed were investigated for stoichiometric methane–air mixtures only [30], burning velocities are measured in the present study for wide ranges of oxygen-enrichment ratio and equivalence ratio. The oxygen-enrichment ratio in the oxidizer Ω is varied from 0.21 (air) to 1.0 (pure oxygen). This enables to vary the flame temperature from $T_b^o = 2261$ K to 3060 K, as shown in Table 2. In this work, three oxygen-enrichment ratios $\Omega = 0.30$, 0.50 and 1.0 are examined and, for each value of Ω, the impact of steam addition is investigated in lean, stoichiometric and rich conditions.

Figure 12 shows the evolution of the laminar flame speed when the water vapor molar fraction is increased from 0 to 0.25, for a stoichiometric ($\phi = 1.0$) slightly oxygen-enriched ($\Omega = 0.30$) mixture. In almost dry conditions ($X_{H_2O} = 0.01$), the measured flame speed s_u reaches 112 cm s^{-1} and fits with numerical predictions. The burning velocity decreases quasi-linearly when the steam molar fraction is increased. The calculations conducted with the two kinetic mechanisms lead to analogue results and a similar quasi-linear decrease of the burning velocity is observed. Experimental and numerical results are in agreement for low steam concentrations $X_{H_2O} < 0.10$. The slope (in absolute value) of the straight line defined by the experimental data is found to be slightly higher than the one associated with the calculated flame speeds. The relative difference η introduced previously reaches about 12% for $X_{H_2O} = 0.20$. This value is lower than that obtained for a wet methane–air stoichiometric mixture ($\Omega = 0.21$), diluted with the same steam concentration $X_{H_2O} = 0.20$. This may indicate that chemical effects of steam addition are reduced for oxygen-enriched flames compared to wet methane–air combustion. Experimental and numerical results obtained in lean ($\phi = 0.70$) and rich ($\phi = 1.40$) conditions for $\Omega = 0.30$ are shown in Fig. 12. In both cases, a similar quasi-linear decrease of the flame speed is observed. In the lean case ($\phi = 0.70$), the agreement between measured and computed flame speeds is within 6%. One can however note that numerical results obtained with Le Cong et al. mechanism slightly underpredict the burning velocity. Despite the slight deviation observed between numerical predictions obtained for steam and virtual species dilutions, it is difficult to discriminate possible chemical effects of water addition because both data sets are enclosed within experimental error bars. In the rich case ($\phi = 1.40$), the numerical predictions of the GRI-mech 3.0 and the experimental results are in good agreement for steam fractions X_{H_2O} varying from 0 to 0.20. In this range of steam concentrations, no significant difference is found between the flame speeds calculated with H_2O and the virtual species Virt-H_2O.

Results are now presented for a higher oxygen concentration $\Omega = 0.50$, for lean ($\phi = 0.6$), stoichiometric ($\phi = 1.0$) and rich ($\phi = 1.5$) mixtures in Fig. 13. As observed previously, the burning velocity decreases linearly with increasing steam molar fraction. Solid and dashed lines indicate the computed burning velocities and show a similar linear dependence with water vapor addition. For lean ($\phi = 0.6$) and stoichiometric ($\phi = 1.0$) mixtures, numerical

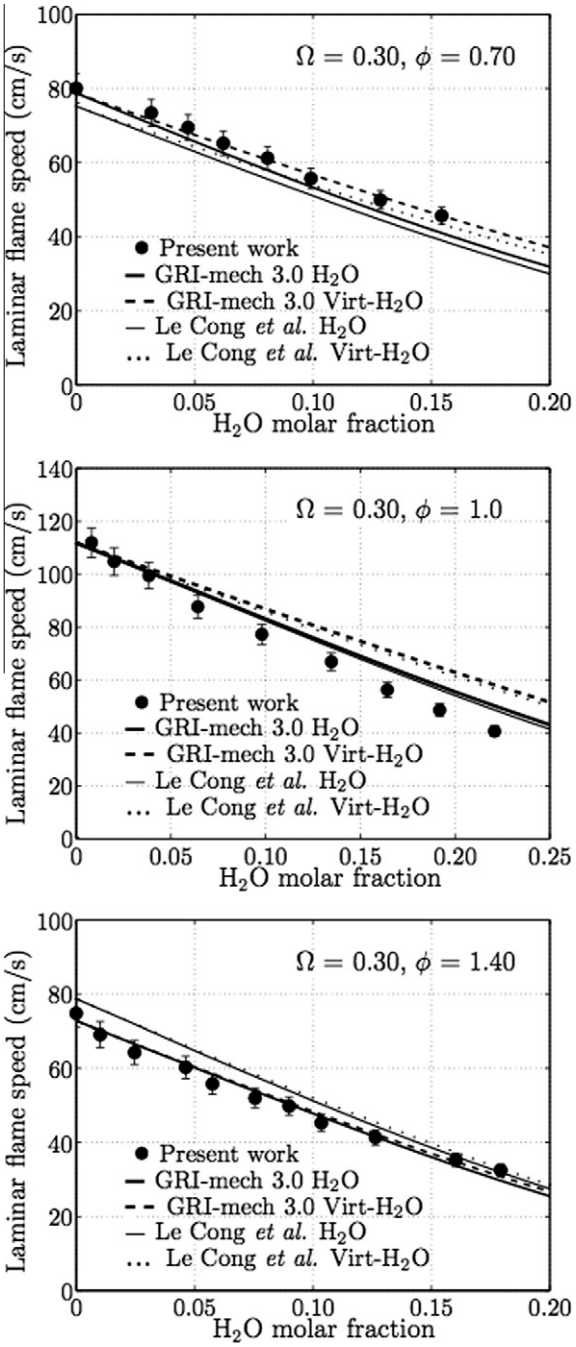

Fig. 12. Experimental (symbols) and computed (lines) laminar flame speeds of $CH_4/O_2/N_2/H_2O$ mixtures, for $\Omega = 0.30$ and $\phi = 0.70$, 1.0 and 1.40, at $T_u = 373$ K and atmospheric pressure.

results obtained with the GRI-mech 3.0 mechanism and the mechanism proposed by Le Cong et al. are very close and match well with the experimental results for the whole range of steam concentrations explored. Furthermore, one can note the deviation between the numerical results obtained with steam addition and those calculated with the virtual species for lean and stoichiometric mixtures. The relative difference η increases with increasing steam molar fraction and reaches 13% for $X_{H_2O} = 0.30$ when $\phi = 0.6$ and 15% for $X_{H_2O} = 0.50$ when $\phi = 1.0$. It is however worth emphasizing that for a given steam molar fraction, the relative difference remains lower than that found for lower oxygen concentrations $\Omega = 0.21$ or 0.30. This confirms that the chemical impact of steam addition on the laminar burning velocity reduces with

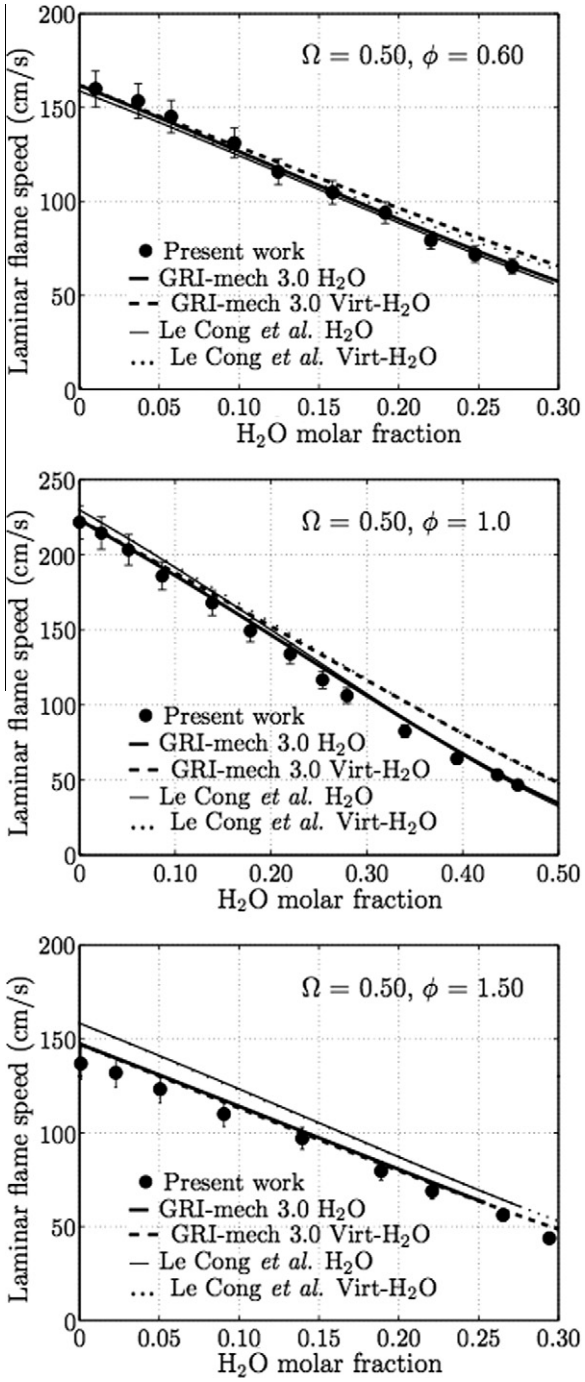

Fig. 13. Experimental (symbols) and computed (lines) laminar flame speeds of $CH_4/O_2/N_2/H_2O$ mixtures, for $\Omega = 0.50$ and $\phi = 0.60$, 1.0 and 1.50, at $T_u = 373$ K and atmospheric pressure.

increasing flame temperature. In rich conditions ($\phi = 1.5$), Le Cong et al. mechanism overpredicts the measured laminar flame speeds by about 10% while predictions based on GRI-mech 3.0 show a better agreement with the measured flame speeds, despite a slight overprediction for dry mixtures. For this equivalence ratio, no chemical effect of steam addition is observed.

Figure 14 shows the flame speeds plotted as a function of the equivalence ratio ϕ, for $\Omega = 0.50$ and for increasing steam molar fractions $X_{H_2O} = 0$, $X_{H_2O} = 0.10$ and $X_{H_2O} = 0.20$. Experimental and numerical results are still in good agreement in the range of conditions explored. In rich conditions, the numerical predictions obtained with Le Cong et al. mechanism are slightly higher than

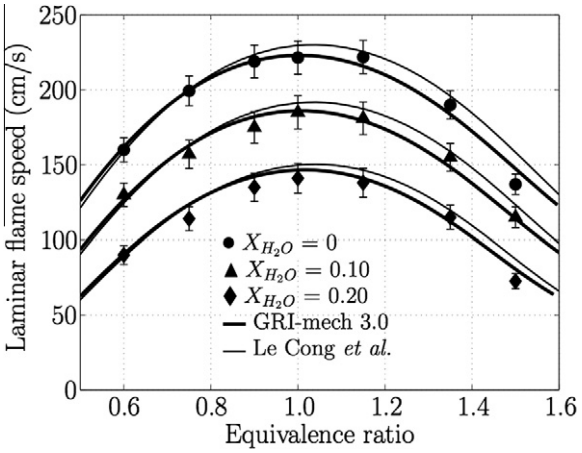

Fig. 14. Experimental (symbols) and computed (lines) laminar flame speeds of $CH_4/O_2/N_2/H_2O$ mixtures as a function of the equivalence ratio ϕ, with $\Omega = 0.50$ and various steam molar fractions $X_{H_2O} = 0$, 0.10 and 0.20, at $T_u = 373$ K and atmospheric pressure.

those calculated with the GRI-mech 3.0 mechanism. This difference reduces with increasing steam concentration.

Finally, flame speeds of steam-diluted methane–oxygen flames ($\Omega = 1.0$) are plotted in Fig. 15, for three equivalence ratios $\phi = 0.5$, 1.0 and 1.50 respectively. For steam molar fractions varying from 0 to 0.45, a good agreement between experimental data and numerical predictions is observed. The flame speed features a linear decrease with increasing steam concentration, which is also well predicted by the simulations performed with the virtual species Virt-H_2O. Results provided by the GRI-mech 3.0 and Le Cong et al. mechanism are similar for $\phi = 0.5$. The latter yields slightly higher burning velocities for $\phi = 1.0$ and 1.5. It is finally remarkable that no significant difference is observed, in these conditions, between the computed flame speeds obtained with H_2O and Virt-H_2O. This highlights that chemical effects of steam dilution on the burning velocity of methane–oxygen flames is negligible. For highly oxygen-enriched flames, the flame speed evolution is mainly due to dilution and thermal effects induced by steam addition.

4.3. Thermal and chemical effects of steam addition

The chemical effect of steam addition on the burning velocity of oxygen-enriched methane flames has been discussed previously, based on the comparison between experimental data and numerical predictions obtained with the virtual species Virt-H_2O. It was shown that, for a fixed steam molar fraction, the chemical effect on the burning velocity reduces when the oxygen-enrichment ratio is increased. This effect, while limited, is however more significant in lean and stoichiometric conditions than in rich conditions. The chemical impact of steam addition is now examined for two mixtures featuring different adiabatic flame temperatures. Results are presented for a stoichiometric methane–air flame $\Omega = 0.21$ and a stoichiometric methane–oxygen flame $\Omega = 1.0$ diluted with a steam molar fraction $X_{H_2O} = 0.20$ or with a virtual species molar fraction $X_{\text{Virt-}H_2O} = 0.20$. The evolution of the molar fraction profiles of H, O, OH and CH_3 radicals in the reaction zone is plotted in Fig. 16. Depending on flame temperature, the presence of water vapor molecules leads to changes in the production and in the consumption of H, O and OH radicals. For a standard methane–air flame ($\Omega = 0.21$) featuring an adiabatic flame temperature $T_b^o \sim 2200$ K, steam addition reduces peak values of H and O atom concentrations respectively by about 30% and 50% compared to the predictions obtained with the virtual species. In contrast, the peak

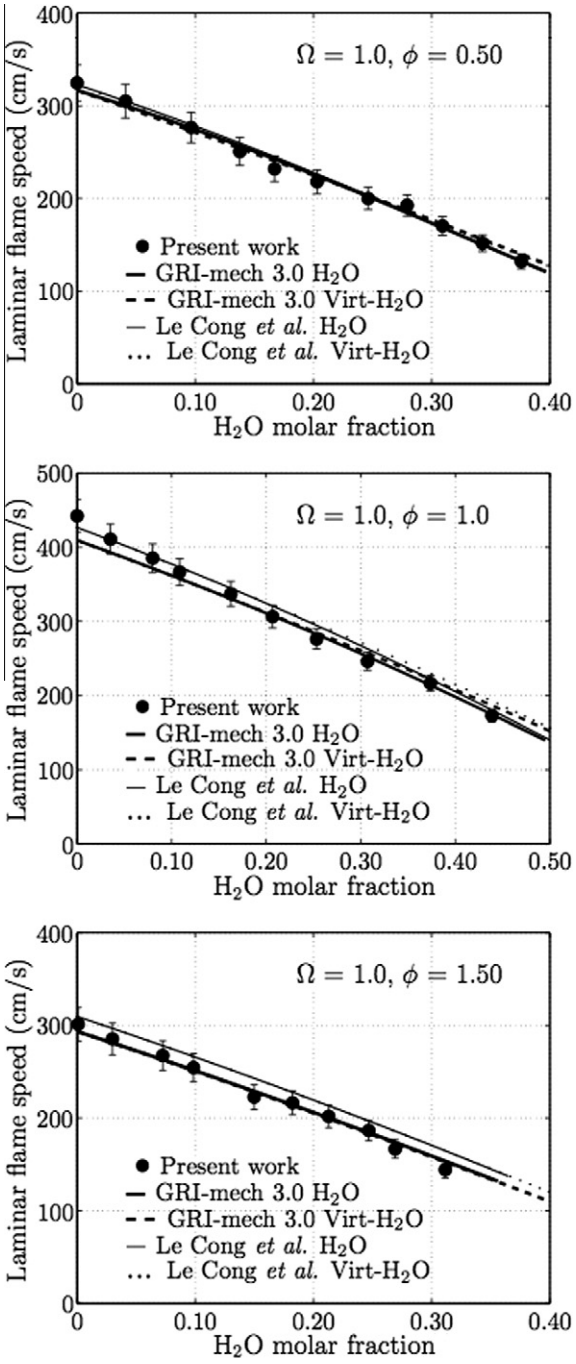

Fig. 15. Experimental (symbols) and computed (lines) laminar flame speeds of $CH_4/O_2/H_2O$ mixtures, for $\Omega = 1.0$ and $\phi = 0.50$, 1.0 and 1.50, at $T_u = 373$ K and atmospheric pressure.

of OH concentration is increased by 17% with steam addition. These observations are consistent with the conclusions reported by Le Cong and Dagaut [24], who attributed this effect to steam high chaperon efficiency in the recombination reaction $H + O_2 + M \rightleftharpoons HO_2 + M$, which competes with the chain-branching reaction $H + O_2 \rightleftharpoons OH + O$. Water vapor addition also favors O radical consumption and OH production in the reaction $H_2O + O \rightleftharpoons OH + OH$, which removes O atoms and tends to inhibit methane oxidation in the reaction $CH_4 + O \rightleftharpoons CH_3 + OH$, especially in lean conditions. For a methane–oxygen flame ($\Omega = 1.0$) featuring an adiabatic flame temperature $T_b^o \sim 3000$ K, H, O and OH concentrations are increased by more than one order of magnitude compared to air combustion. This increase is due to the high flame temperature

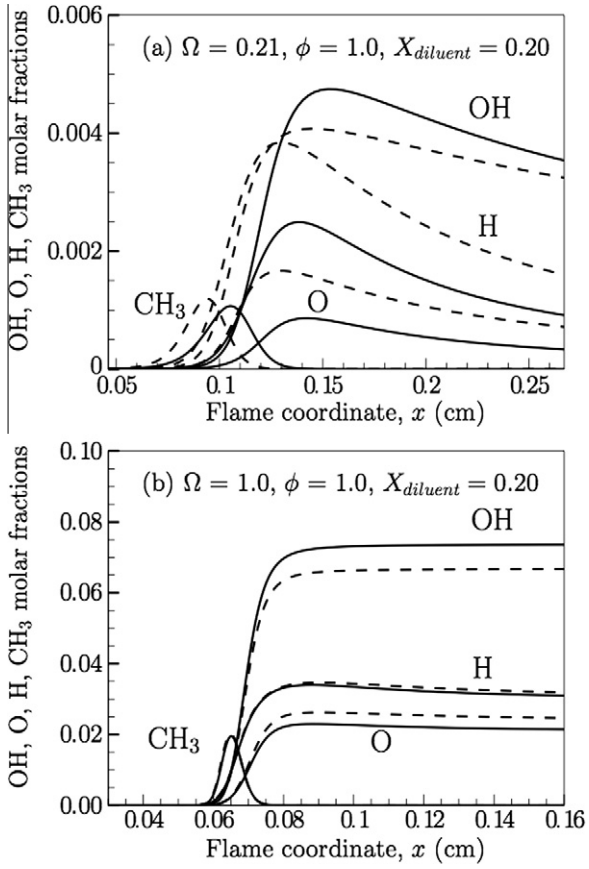

Fig. 16. Profiles of OH, O, H and CH_3 molar fractions in one-dimensional $CH_4/O_2/N_2/H_2O$ stoichiometric flames computed with the GRI-mechanism 3.0. Continuous lines: diluent = H_2O; Dashed lines: diluent = Virt-H_2O. (a) $\Omega = 0.21$ (air), $\phi = 1.0$, $X_{diluent} = 0.20$; (b) $\Omega = 1.0$ (oxygen), $\phi = 1.0$, $X_{diluent} = 0.20$.

obtained with pure oxygen combustion. The chemical effect of water vapor is here considerably reduced. In this case, the differences in H, O and OH radical concentrations calculated with H_2O and Virt-H_2O dilutions are limited.

The evolution of the flame speed with steam addition $s_u(X_{H_2O})$ is now analyzed by plotting in Fig. 17 the ratio $s_u(X_{H_2O})/s_u(X_{H_2O} = 0)$, where $s_u(X_{H_2O} = 0)$ is the flame speed of the dry mixture, for various oxygen-enrichment ratios and equivalence ratios.

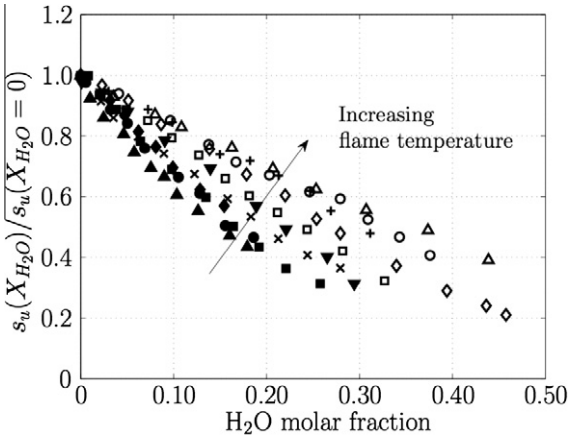

Fig. 17. Laminar flame speed ratio $\bar{s}_u(X_{H_2O})/\bar{s}_u(X_{H_2O} = 0)$ of $CH_4/O_2/N_2/H_2O$ mixtures, at $T_u = 373$ K and atmospheric pressure. (•) $\Omega = 0.21$, $\phi = 1.0$; (♦) $\Omega = 0.30$, $\phi = 0.70$; (■) $\Omega = 0.30$, $\phi = 1.0$; (▲) $\Omega = 0.30$, $\phi = 1.40$; (×) $\Omega = 0.50$, $\phi = 0.60$; (□) $\Omega = 0.50$, $\phi = 0.75$; (◇) $\Omega = 0.50$, $\phi = 1.0$; (▼) $\Omega = 0.50$, $\phi = 1.50$; (○) $\Omega = 1.0$, $\phi = 0.50$; (△) $\Omega = 1.0$, $\phi = 1.0$; (+) $\Omega = 1.0$, $\phi = 1.50$.

Experimental results show that, for all mixture compositions explored, the ratio $s_u(X_{H_2O})/s_u(X_{H_2O}=0)$ features a quasi-linear decrease with increasing steam molar fraction. The rate of decrease of this ratio reduces globally with increasing oxygen-enrichment ratio. For a given oxygen-enrichment ratio, the lowest rate of decrease of this ratio is systematically obtained for the stoichiometric mixture. These observations suggest that the decrease rate of the flame speed is mainly controlled by the adiabatic flame temperature. This conjecture is used in Appendix A to build a semi-empirical model for the flame speed evolution with steam dilution. This model, based on a one-step overall reaction, provides an analytical expression for the ratio $s_u(X_{H_2O})/s_u(X_{H_2O}=0)$ as a function of steam molar fraction X_{H_2O}. Although based on crude assumptions, this analytical model can be used to quickly estimate the laminar burning velocity of steam-diluted oxygen-enriched mixtures by means of thermo-chemistry calculations.

5. Conclusion

The effects of water vapor addition on the laminar burning velocity of oxygen-enriched methane flames were investigated experimentally and numerically. A large set of results was obtained for preheated dry and wet mixtures at $T_u = 373$ K and at atmospheric pressure $p_u = 1$ bar. Burning velocities were measured for equivalence ratios ranging from 0.50 to 1.50, oxygen-enrichment ratios varying from $\Omega = X_{O_2}/(X_{O_2}+X_{N_2}) = 0.21$ (air–fuel combustion) to 1.0 (oxy–fuel combustion) and steam molar fractions covering $X_{H_2O} = 0$ to 0.45 in $CH_4/O_2/N_2/H_2O$ mixtures. Covering this large range of operating conditions was made possible by using a specific experimental facility dedicated to premixed oxy–fuel combustion, including a newly devised humidifier for steam production and different converging nozzles. Laminar flame speeds were determined from steady conical flames with the flame area method. Experimental results were compared to computed laminar burning velocities using the detailed kinetic mechanism GRI mech. 3.0 and the kinetic mechanism developed by Le Cong and Dagaut for methane oxidation in presence of water vapor. The major conclusions of the present study are:

1. Humidifiers, based on membrane permeation technologies and equipped with a closed loop control of humidity, are flexible and efficient solutions to obtain a precise control of steam concentration in a carrier gas for a wide range of operating conditions and steam dilution rates.
2. The burning velocity of methane flames decreases when the water vapor concentration is increased. This decrease is quasi-linear with increasing steam molar fraction, especially for highly oxygen-enriched flames. This evolution is well predicted by the two detailed kinetic mechanisms used in this study (GRI-mech 3.0 and Le Cong et al. mechanisms), except for methane–oxygen flames with low steam dilution rates ($X_{H_2O} < 0.10$) where the burning velocity is slightly underestimated by numerical predictions.
3. Steam addition has a significant chemical effect on the burning velocity of wet methane–air flames. This impact is found to be greater in lean and near-stoichiometric conditions than in rich conditions, and strongly reduces when the oxygen concentration is increased. In the case of oxygen-enriched reactive mixtures, steam can be considered as an inert diluent, even at high steam concentrations.

These findings are of interest for the development of oxy-combustion technologies with flue gas recirculation, as considered for example for CO_2 capture and storage. In this type of highly reactive mixtures, water vapor may essentially be treated as an inert diluent.

Acknowledgments

This research was supported by Air Liquide under the technical monitoring of Dr. B. Labégorre and Dr. R. Tsiava, and by the French National Agency for Research and Technology (*Agence Nationale pour la Recherche et la Technologie*) under a doctoral grant. The authors thank Dr. K. Gurubaran for his valuable help in PIV measurements. The technical support provided by J. Beaunier, S. El-Ghazi, E. Jean-Bart and Y. Le Teno is also acknowledged.

Appendix A. A simplified model for inert diluent addition

Neglecting the chemical effects of steam addition on the burning velocity of oxygen-enriched methane flames, it is possible to describe the evolution of the ratio $s_u(X_{H_2O})/s_u(X_{H_2O}=0)$ with a simplified model based on a one-step overall reaction:

$$\nu_F F + \nu_O O + \nu_I I \rightleftharpoons \sum_k \nu_k P_k + \nu_I I \tag{A.1}$$

where fuel, oxygen and inert diluent are designated by the letters F, O and I respectively, while the notation P_k encompasses reaction products. The diluted versus non-diluted molar fraction ratio $X_j(\nu_I)/X_j(\nu_I=0)$ calculated either for the fuel (j = F) or for the oxidizer (j = O) only depends on the inert diluent molar fraction X_I:

$$\frac{X_j(\nu_I)}{X_j(\nu_I=0)} = \frac{\nu_F+\nu_O}{\nu_F+\nu_O+\nu_I} = (1-X_I) \tag{A.2}$$

The mass burning flux, defined as $f_u^o = \rho_u s_u^o$, is a function of the exothermicity, diffusivity and reactivity of the mixture. In the limit of high activation energy, it is possible to obtain the following expression for the mass burning flux [48]:

$$\left(f_u^o\right)^2 = \left(\frac{1}{Ze}\right)^2 Le \frac{\lambda}{c_p}\dot{\omega} \tag{A.3}$$

where λ and c_p are the thermal conductivity and the heat capacity of the mixture, and $\dot{\omega}$ is the overall reaction rate. We further assume that this reaction rate can be modeled by an Arrhenius law $\dot{\omega} = A X_F^{n_F} X_O^{n_O} \exp(-T_a/T_b^o)$ where A is a pre-exponential factor, n_F and n_O denote the fuel and oxidizer specific reaction orders, $T_a = E_a/R$ corresponds to the activation temperature and T_b^o indicates the burned gases temperature. The laminar flame speed s_u^o is then given by:

$$s_u^o = \frac{1}{\rho_u Ze}\left(Le\frac{\lambda}{c_p}\right)^{\frac{1}{2}}\left[A X_F^{n_F} X_O^{n_O} \exp\left(\frac{-T_a}{T_b^o}\right)\right]^{\frac{1}{2}} \tag{A.4}$$

Assuming that the variations of λ, Le and T_a remain limited when the inert diluent molar fraction is increased, an expression for the flame speeds ratio $s_u^o(X_I)/s_u^o(X_I=0)$ can be derived from Eqs. (A.2) and (A.4):

$$\frac{s_u^o(X_I)}{s_u^o(X_I=0)} \simeq \frac{(Ze\rho_u\sqrt{c_p})_{X_I=0}}{(Ze\rho_u\sqrt{c_p})_{X_I}}(1-X_I)^{(n_F+n_O)/2} \times \exp\left[\frac{-T_a}{2T_b^o(X_I)}\left(1-\frac{T_b^o(X_I)}{T_b^o(X_I=0)}\right)\right] \tag{A.5}$$

Noting that the Zeldovich number can be approximated by $Ze \sim T_a/T_b^o$ for oxygen-enriched flames and defining a reduced flame temperature $\widetilde{T}(X_I) = T_b^o(X_I)/T_b^o(X_I=0)$, Eq. (A.5) yields:

$$\frac{s_u^o(X_I)}{s_u^o(X_I=0)} \sim \frac{(\rho_u\sqrt{c_p})_{X_I=0}}{(\rho_u\sqrt{c_p})_{X_I}}(1-X_I)^{n/2}\widetilde{T}(X_I) \times \exp\left[\frac{-T_a}{2T_b^o(X_I)}\left(1-\widetilde{T}(X_I)\right)\right] \tag{A.6}$$

where $n = n_F + n_O$ is the overall reaction order. Eq. (A.6) provides a simple expression for the ratio $s_u^o(X_I)/s_u^o(X_I = 0)$, which is a function of the inert diluent molar fraction X_I, the density ρ_u and the heat capacity c_p of the unburned gases, the activation temperature T_a, the reduced flame temperature $\tilde{T}(X_I)$ and the overall reaction order n. For highly oxygen-enriched mixtures, the ratio $T_a/T_b^o(X_I)$ decreases and the reduced flame temperature $\widetilde{T}(X_I)$ remains close to unity. In these conditions, the exponential term in Eq. (A.6) can then be replaced by unity, indicating that the reduced flame speed $s_u^o(X_I)/s^o(X_I = 0)$ is proportional to the reduced flame temperature $\widetilde{T}(X_I)$.

References

[1] D.L. Zhu, F.N. Egolfopoulos, C.K. Law, Proc. Combust. Inst. 22 (1988) 1537–1545.
[2] F.S. Liu, H.S. Guo, G.J. Smallwood, Combust. Flame 133 (4) (2003) 495–497.
[3] H. Kobayashi, H. Hagiwara, H. Kaneko, Y. Ogami, Proc. Combust. Inst. 31 (2007) 1451–1458.
[4] T. Le Cong, P. Dagaut, Combust. Sci. Technol. 180 (2008) 2046–2091.
[5] T. Le Cong, P. Dagaut, Proc. Combust. Inst. 32 (2009) 427–435.
[6] T.F. Wall, Proc. Combust. Inst. 31 (2007) 31–47.
[7] J.D. Figueroa, T. Fout, S. Plasynski, H. McIlvried, R.D. Srivastava, Int. J. Greenhouse Gas Control 2 (1) (2008) 9–20.
[8] F. Dryer, Proc. Combust. Inst. 16 (1) (1977) 279–295.
[9] T. Miyauchi, Y. Mori, T. Yamaguchi, Proc. Combust. Inst. 18 (1) (1981) 43–51.
[10] G.L. Touchton, J. Eng. Gas Turbines Power – Trans. ASME 107 (3) (1985) 706–713.
[11] L.G. Blevins, R.J. Roby, An experimental study of NO_x reduction in laminar diffusion flames by addition of high levels of steam, in: ASME Paper 95-GT-327, 1995.
[12] J.-L. Meyer, G. Grienche, An experimental study of steam injection in an aeroderivative gas turbine, in: ASME Paper 97-GT-506, 1997.
[13] S.M. Correa, Proc. Combust. Inst. 27 (1998) 1793–1813.
[14] A. Bhargava, M. Colket, W. Sowa, K. Casleton, D. Maloney, J. Eng. Gas Turbines Power – Trans. ASME 122 (3) (2000) 405–411.
[15] B. de Jager, J.B.W. Kok, G. Skevis, Proc. Combust. Inst. 31 (2007) 3123–3130.
[16] M.J. Landman, M.A.F. Derksen, J.B.W. Kok, Combust. Sci. Technol. 178 (4) (2006) 623–634.
[17] S.P. Fuss, E.F. Chen, W.H. Yang, R.J. Kee, B.A. Williams, J.W. Fleming, Proc. Combust. Inst. 29 (2002) 361–368.
[18] G.O. Thomas, Combust. Flame 130 (1–2) (2002) 147–160.
[19] G.T. Linteris, L. Truett, Combust. Flame 105 (1–2) (1996) 15–27.
[20] A. Kusharin, O. Popov, G. Agafonov, Proc. Combust. Inst. 26 (1996) 985–991.
[21] A.Y. Kusharin, O.E. Popov, G.L. Agafonov, B.E. Gelfand, Exp. Therm. Fluid Sci. 21 (1–3) (2000) 2–8.
[22] R. Seiser, K. Seshadri, Proc. Combust. Inst. 30 (1) (2005) 407–414.
[23] C.S. Yoo, S.D. Lee, S.H. Chung, Combust. Sci. Technol. 155 (2000) 227–242.
[24] T. Le Cong, P. Dagaut, Effect of water vapor on the kinetics of combustion of hydrogen and natural gas: experimental and detailed modeling study, in: ASME Paper GT 2008-50272, Berlin, Germany, 2008.
[25] D.D.S. Liu, R. MacFarlane, Combust. Flame 49 (1983) 59–71.
[26] G. Koroll, S. Mulpuru, Proc. Combust. Inst. 21 (1986) 1811–1819.
[27] A.K. Das, K. Kumar, C.J. Sung, Combust. Flame 158 (2) (2011) 345–353.
[28] Y.N. Shebeko, S.G. Tsarichenko, A.Y. Korolchenko, A.V. Trunev, V.Y. Navzenya, S.N. Papkov, A.A. Zaitzev, Combust. Flame 102 (4) (1995) 427–437.
[29] M. Kuznetsov, R. Redlinger, W. Breitung, J. Grune, A. Friedrich, N. Ichikawa, Proc. Combust. Inst. 33 (1) (2011) 895–903.
[30] V.S. Babkin, A.V. V'yun, Fiz. Goreniya Vzryva 7 (3) (1971) 392–395.
[31] G.S. Settles, Schlieren and Shadowgraph Techniques, Springer, Berlin, 2001.
[32] B. Lewis, G. Von Elbe, Combustion, Flames and Explosions of Gases, third ed., Academic Press Inc., Orlando, 1987.
[33] J. Kee, K. Grcar, M. Smooke, J. Miller, PREMIX: A FORTRAN Program for Modelling Steady Laminar One-dimensional Premixed Flames, Technical Report, Sandia National Laboratories, 1985.
[34] G.P. Smith, D.M. Golden, M. Frenklach, N.W. Moriarty, B. Eiteneer, M. Goldenberg, C.T. Bowman, R.K. Hanson, S. Song, W.C. Gardiner, Jr., V.V. Lissianski, Z. Qin, <http://www.me.berkeley.edu/gri_mech/>.
[35] F.S. Liu, H.S. Guo, G.J. Smallwood, O.L. Gulder, Combust. Flame 125 (2001) 778–787.
[36] C.K. Law, Combustion Physics, Cambridge University Press, 2006.
[37] G.E. Andrews, D. Bradley, Combust. Flame 18 (1972) 133–153.
[38] M. Matalon, Combust. Sci. Technol. 31 (1983) 169–181.
[39] P. Clavin, Prog. Energy Combust. Sci. 11 (1985) 1–59.
[40] C.K. Wu, C.K. Law, Proc. Combust. Inst. 20 (1984) 1941–1949.
[41] C.K. Law, Proc. Combust. Inst. 22 (1988) 1381–1402.
[42] G. Dixon-Lewis, Proc. Combust. Inst. 23 (1990) 305–324.
[43] J.H. Tien, M. Matalon, Combust. Flame 84 (1991) 238–248.
[44] A. Van Maaren, D.S. Thung, L.P.H. de Goey, Combust. Sci. Technol. 96 (1994) 327–344.
[45] C. Vagelopoulos, F. Egolfopoulos, C. Law, Proc. Combust. Inst. 25 (1) (1994) 1341–1347.
[46] B.H. Chao, F.N. Egolfopoulos, C.K. Law, Combust. Flame 109 (1997) 620–638.
[47] C.M. Vagelopoulos, F.N. Egolfopoulos, Proc. Combust. Inst. 27 (1998) 513–519.
[48] C.K. Law, C.J. Sung, Prog. Energy Combust. Sci. 26 (2000) 459–505.
[49] A.P. Kelley, C.K. Law, Combust. Flame 156 (2009) 1844–1851.
[50] J.M. Truffaut, G. Searby, Combust. Sci. Technol. 149 (1–6) (1999) 35–52.
[51] J. Bechtold, M. Matalon, Combust. Flame 67 (1) (1987) 77–90.
[52] I. Sochet, M. Aminallah, J. Brossard, Shock Waves 7 (3) (1997) 163–174.
[53] C. Matignon, D. Desbordes, H.N. Presles, C.R. Mec. 334 (4) (2006) 238–242.
[54] J.E. Shepherd, Proc. Combust. Inst. 32 (2009) 83–98.
[55] M.J. Remie, M.F.G. Cremers, K.R.A.M. Schreel, L.P.H. de Goey, Combust. Flame 147 (2006) 163–170.
[56] I. Glassman, Combustion, third ed., Academic Press, San Diego, CA, 1996.
[57] D. Dunn-Rankin, F. Weinberg, Combust. Flame 113 (1998) 303–311.
[58] D. Durox, S. Ducruix, Combust. Flame 120 (2000) 595–598.
[59] C.W. Choi, I.K. Puri, Combust. Flame 126 (3) (2001) 1640–1654.
[60] C.J. Sun, C.J. Sung, L. He, C.K. Law, Combust. Flame 118 (1999) 108–128.
[61] G. Joulin, T. Mitani, Combust. Flame 40 (1981) 235–246.
[62] M.I. Hassan, K.T. Aung, G.M. Faeth, Combust. Flame 115 (1998) 539–550.
[63] K.J. Bosschaart, L.P.H. de Goey, Combust. Flame 136 (2004) 261–269.
[64] Y.F. Dong, C.M. Vagelopoulos, G.R. Spedding, F.N. Egolfopoulos, Proc. Combust. Inst. 29 (2002) 1419–1426.